Electrical Versus Optical Generation of Leader Signals for Downconversion Leader-Follower Optical Coherence Tomography

Alejandro Martinez Jimenez, Ramona Cernat, and Adrian Podoleanu, *Senior Member, IEEE*

***Abstract*—The paper refers to advancements in the production of *en-face* optical coherence tomography (OCT) images from different depths in a sample in real time, using Downconversion Leader-Follower optical coherence tomography method. So far, for a sample placed in an interferometer (Follower), all previous Downconversion Leader-Follower reports employed an interferometer (Leader) to determine the depth where the OCT signal is selected from. In this paper, for the first time, the Leader interferometer is replaced by an arbitrary waveform generator, i.e., optical generation of the reference signal to perform downconversion is replaced by electrical synthesis. In this way, *en-face* images from different depths are presented in real time, without recurring to a second interferometer. Avenues opened by electrical synthesis of signals otherwise provided by interferometers are discussed, with potential to be adopted in signal processing, manipulation and presentation of high-resolution images in orthogonal orientations to serve better diagnosis.**

***Index Terms*—*en-face* optical coherence tomography, downconversion, leader-follower OCT, simultaneous imaging at multiple depths.**

Received 4 November 2025; revised 10 December 2025; accepted 13 December 2025. Date of publication 22 December 2025; date of current version 19 January 2026. The work of Alejandro Martinez Jimenez and Adrian Podoleanu was supported by Engineering and Physical Sciences Council (EPSRC) of the U.K. for FoVEnOCT, under Grant EP/X000125/1. The work of Ramona Cernat, Alejandro Martinez Jimenez, and Adrian Podoleanu was supported by European Commission through ITN GA under Grant GA860807 (NETLAS). The work of Ramona Cernat and Adrian Podoleanu was supported by NIHR MOORFIELDS BRC, BRC3 and in part by NIHR under Grant BRC4-05-RB413-302, Imaging, Visual Assessment & Digital Innovation, at Moorfields Eye Hospital NHS FT and UCL Institute of Ophthalmology. The work of Adrian Podoleanu was supported in part by U.K.'s Biotechnology and Biological Sciences Research Council (BBSRC) under Grant 5DHiResE (BB/S016643/1) and Grant BB/X003744/1, in part by the Impact Acceleration Accounts IAA-BBSRC, under Grant BBSRC BB/X511158/1 and Grant IAA-MRC MR/X502753/1, in part by NIHR under Grant 202879 at King's College and Moorfields Eye Hospital, and in part by DPFS MRC 662915 to UoNottingham and UoKent. Alejandro Martinez Jimenez also acknowledges support for a Beatriz Galindo junior fellowship (BG24/00089) from the Spanish Ministry of Science, Innovation and Universities and from the University of Castilla La-Mancha. *(Alejandro Martinez Jimenez and Ramona Cernat contributed equally to this work.) (Corresponding author: Adrian Podoleanu.)*

Alejandro Martinez Jimenez is with the Applied Optics Group, School of Engineering, Mathematics and Physics, University of Kent, CT2 7NH Canterbury, U.K., and also with Departamento de Física, Universidad de Castilla La-Mancha, Campus Fábrica de Armas, 45004 Toledo, Spain (e-mail: alejandro.mjimenez@uclm.es).

Ramona Cernat and Adrian Podoleanu are with the Applied Optics Group, School of Engineering, Mathematics and Physics, University of Kent, CT2 7NH Canterbury, U.K. (e-mail: rc72@kent.ac.uk; a.g.h.podoleanu@kent.ac.uk).

This article has supplementary downloadable material available at https://doi.org/10.1109/JPHOT.2025.3646935, provided by the authors.

Digital Object Identifier 10.1109/JPHOT.2025.3646935

I. Introduction

THE conventional method of swept source (SS) optical coherence tomography OCT [1] employs a high frequency rate digitizer and a Fourier Transform (FT) block [2]. Generally, due to nonlinear sweeping and dispersion in the OCT interferometer, the spectrum modulation is not regular, more conventionally referred to as exhibiting a chirp. In conventional FT based SSOCT, for each sweep, data need to be organized in equal slots along the wavenumber coordinate before the FT. A FT block processes the digitized electrical signal delivered by the photodetector to obtain an A-scan (a reflectivity profile in depth in the sample imaged). There has been a tremendous progress in the last 5 years in tuning extremely fast, so fast, that signal processing cannot be completed in a sweeping interval.

In addition, employing a conventional OCT system [1], [2] based on a FT processor, to produce an *en-face* OCT image, all A-scans for all lateral pixels need to be acquired first, followed by assembly of the A-scans into a volume of the object. Only then via a software cut of the volume at the depth required, an *en-face* OCT slice can be delivered.

The two reasons above, limitation of tuning rate due to need to complete signal processing on each sweep and the fact that *en-face* slicing can only be produced by the end of volume acquisition, via a software cut of the volume of data, have determined us to look to other signal processing modalities to process the information encoded onto the spectrum modulation at the OCT interferometer output. To this goal, the Leader Follower (LF) method was introduced [3]. This does not employ a FT processor, but a processor for each optical path difference (OPD) of interest, operating on comparing the spectrum with stored shapes in the computer memory, termed as masks. The masks represent shapes of the same spectrum for different OPD values when the sample is replaced with a mirror. The LF method required experimental acquisition of spectral shapes using a mirror as sample, for many values of OPD in the interferometer. The LF method was improved by realising that such spectral shapes, referred as masks, can be calculated from at least two experimentally collected spectra at the interferometer output for two OPD values [4]. A minimum of two only, as the phase of the interference signal depends on two unknown functions, $g(k)$, describing the tuning nonlinearity and $h(k)$ the dispersion in the interferometer, where k is the wavenumber. Once these two functions are derived, any mask, for any OPD of interest

can be calculated. The algorithm developed to calculate such masks eliminated the need for many experimental acquisitions of spectra to be used as masks and offered more stability to phase fluctuations by calculating complex masks, hence denomination of the method as complex leader follower (CLF).

The mask can also be produced by using an interferometer, in which case the processor for each OPD can be reduced from a high speed digitiser to an analog mixer [5], [6], followed by a much lower speed digitiser. This diminishes the demand for the sampling rate of the signal employed via the downconversion operation performed by the mixer, hence the method was termed Downconversion Leader Follower (DLF). In continuation, we will refer to the method used in [5], [6] as optical-optical (OO) DLF, where an interferometer [5] or two interferometers [6] were used to generate the masks, i.e., by optical means. As another advantage of the downconversion method, is the direct provision of *en-face* OCT images.

The core principle of LF, CLF and OO DLF is based on comparison of patterns of modulation in the spectrum at the interferometer output. In LF, CLF and OO DLF the chirp due to *g(k)* and *h(k)* is incorporated into the mask (experimentally produced in LF and OO DLF or calculated in the CLF). Extra processing, such as resampling [7] or using a clock when employing the conventional FT based processing are not needed.

The DLF method is the subject of the current paper. DLF was originally introduced based on a physical Leader interferometer (LI) in addition to the main OCT interferometer referred here as the Follower interferometer (FI), where the FI incorporates a lateral scanner for scanning the sample. Both interferometers are driven by the same swept source. Any point in depth in the object placed in the FI is selected by the OPD value in the LI. This is why such a method was initially called Master – Slave, terminology recently abandoned for a more inclusive reference, as Leader-Follower[1] ∗.

A new method of DLF is presented in this paper, referred from now on as electrical-optical (EO) DLF. For the first time, we propose to replace the optical generation of the pattern to be used as mask with electrical synthesis. At a glance, the signal generated should manifest more phase stability than that delivered by an optical interferometer in OO DLF. The phase stability characterising the electrical generation of masks can only be replicated if the Leader interferometer is assembled as a common path interferometer. A common path interferometer manifests less phase fluctuations than a simple Michelson or Mach Zehnder interferometer with exposed long arms to air fluctuations. When implemented in fibre, Michelson or Mach Zehnder interferometer are subject to thermal fluctuations. However a common path interferometer is less versatile in scanning the OPD. Electrical synthesis, in addition to better phase stability offers high versatility in generating masks corresponding to different OPD values. In addition, combining electrical synthesis with electrical mixing leads to a new versatile tool in OCT signal processing.

[1] ∗In this report, the authors decided to replace the Master – Slave (MS) terminology used in previous reports, including [3], [4], [5]. [6], [10], [13], [15], [19] and [22] with the more inclusive terminology of Leader -Follower (LF) and Complex Master Slave as Complex Leader – Follower method (CLF).

The process of multiplication of the signal produced by the Follower Interferometer with the signal delivered by each Leader Interferometer adjusted on a different OPD [5], [6] was obtained by using a separate mixer for each Leader Interferometer. An in-phase and quadrature (*I&Q*) active mixer [8] which consists of two mixers was employed. Each mixer does a multiplication of the signals at their two inputs, radio frequency (RF) and local oscillator (LO). The signal at the RF input is multiplied in-phase with that applied at the LO input in one of the mixers, with output *I*, and the second mixer multiplies the RF with a quadrature copy of LO (shifted in phase by 90°), with output *Q*. By calculating the square of each of the two *I* and *Q* outputs and adding them up, a signal with amplitude tolerant to phase fluctuations between the signals applied to the two inputs of the *I&Q* mixer is achieved.

In this paper, in order to implement downconversion, a similar active mixer is used as already reported [6]. However here, optical production of Leader signals using interferometers is replaced by electrical synthesis, using arbitrary waveform generators. The DLF performance is analysed in terms of signal decay with depth and axial resolution achieved. This study demonstrates that electrical synthesis of the mask can lead to similar performance to that achieved using interferometers, with the immediate advantage of less optics complexity, more compact implementation and supplementary versatility in choosing the depth of images displayed.

This report constitutes a proof of concept which if developed further, may lead to many more OCT signals being delivered simultaneously from different depths, where a large number of LIs is replaced by the same number of electrical generators (Table I in Discussion section). Obviously, it would be difficult to increase the number of A-scan points by employing the same number of interferometers, as LIs. Otherwise, an immediate application of the EO DLF presented here is in the provision of an *en-face* image or of a few such *en-face* images using an add-on electronic block to any swept source optical coherence tomography (SSOCT) system. The only alteration to an existent SSOCT system is to tap into the photodetected signal and into the trigger from the swept source. No division of optical power is required either, as necessary for OO DLF using physical interferometers, leading to superior sensitivity for the EO DLF, especially when power from the swept source is limited. However, the proof of concept of this study is not just limited to OCT, the core concept of using a synthetic signal may be extended for different metrology technologies, such as in frequency scanning interferometry [9], where a stable length controller, typically a second optical interferometer is needed, and therefore a synthetic signal could replace it.

II. Theory

In the SSOCT practice, the depth information of a scattering center is coded into the modulation of the channeled spectrum at the OCT interferometer output, translated into the temporal photodetected signal, *C(k),* during each sweep. In SSOCT, the channeled spectrum, *C(k)*, where k represents the wavenumber, for each sweep, is processed to obtain a reflectivity in depth in the sample, i.e., an A-scan, along the spatial coordinate *z*.

In conventional SSOCT, the ubiquitous signal processing from wavenumber, k, to space, z, consists in a Fourier Transform (FT) of the photodetected signal, $C(k)$. This is described by an integration over the spectral domain, i.e., versus wavenumber k between the edges of the tuned spectrum, $k_{\min}$ and $k_{\max}$, of the product between $C(k)$ and exponential factors, parts of the FT calculation. In digital form, this can be described by:

$$A(z) = \sum_{k_{\min}}^{k_{\max}} C(k) \cdot e^{ikz} \tag{1}$$

In general, tuning manifests nonlinearity, i.e., the variable k is not proportional to the time coordinate. This imprints a chirp versus k in the channeled spectrum $C(k)$. Therefore, for a single surface object, a mirror, the channeled spectrum modulation is not a strict sinusoidal function. In addition, dispersion in the interferometer may also induce a chirp. Therefore, before applying the FT in (1), the data $C(k)$ is reorganized to exhibit a linear phase versus the k variable, i.e., data are either read with a clock, usually supplied by the swept source or data are resampled along equal wavenumber slots [10].

A. The Three Versions of Leader Follower OCT Method: Leader Follower (LF), Complex Leader Follower (CLF) and Downconversion Leader Follower (DLF)

The paper is on a novel method of DLF. However, in order to present the novel DLF method, we refer in this section to the signal processing of different earlier versions of the LF methods, from which the DLF has been derived. The CLF method [4] operates differently than (1), where a similar average is calculated, however with the data as it is, but using chirped exponentials:

$$A(z) = \sum_{k\ =k_{\min}}^{k_{\max}} C(k) \cdot e^{i[g(k)z+h(k)]} \tag{2}$$

In the CLF practice, the exponentials, are called masks and are described by:

$$M_z(k) = e^{i[g(k)z+h(k)]} \tag{3}$$

where the function $g(k)$ describes the tuning curve versus k, performed by the swept source and $h(k)$ represents dispersion in the interferometer. For a linearly sweeping source, $g(k) = k$. Initially, the LF method was applied using stored versions [3] of the channeled spectra experimentally acquired for different OPD/2 $= z$ values, representing real parts of the masks in (3). Later on, it was realized that all masks, in their complex form in (3) for all needed values z along the reflectivity profile, A-scan in the sample, can be obtained from at least two experimental channeled spectra, at two different OPD values, that allow calculation of the two functions, $g(k)$ and $h(k)$. Based on the two functions $g(k)$ and $h(k)$ so inferred, a complex version of the LF protocol [4] was devised, CLF, where complex masks for any values z of interest are calculated. In short, the FT based methods as well as the LF and CLF methods rely on calculation of spectral averages of a product of two functions. For the FT based SSOCT, the two functions in the product are a modified version of the data acquired, $C(k)$ and a base of monochromatic exponentials. For LF and CLF based SSOCT, the two functions in the product are the data acquired, $C(k)$ as they are, and either the real forms of masks of (3) (experimentally acquired for each OPD of interest) in LF or calculated complex forms of masks for each OPD of interest in CLF. The manipulation of the two functions is an active field of research, where fractional OCT has been proposed [11] or optical computing [12] in an effort to decode the modulation imprinted into the spectrum at the interferometer output independent of nonlinearity in reading the spectrum or the dispersion left uncompensated.

The (1) has been implemented in the practice of conventional OCT by using digital calculation of the signal measured spectrally, by both methods of spectrometer based OCT and swept source based OCT. Equally, the (2) has also been implemented in practice of LF and DLF by using digital calculation of the signal measured spectrally, by both methods of spectrometer based OCT and swept source based OCT. Calculations of such products require sampling of the $C(k)$ signal, hence high speed digitizers.

A 3rd LF method reported is downconversion leader follower (DLF). In DLF [5], [6], the product calculation and average described by (2) are replaced by an analog mixer and a low pass filter. In this way a much lower sampling rate digitizer is needed.

In conclusion all three procedures, FT based, LF (and complex LF) based, as well as the DLF operate an average (inner product) of the type:

$$A(z) = \langle C(k) M_z(k) \rangle \tag{4}$$

In FT based conventional OCT processing, as well as in LF and CLF, the average in (4) is calculated over the time interval of the sweeping by digital means. In DLF, analog means are used, by employing a mixer followed by a low pass filter. For FT based conventional OCT processing, $C(k)$ is a resampled version of the data and the mask in (4) is the exponential in (3) where $h(k) = 0$ and $g(k) = k$.

In this paper there will be often references to the calculation of the average in (4). In previous DLF implementations, the masks were produced using another interferometer (Leader) [5] or two LIs [6]. This study is dedicated to an alternative DLF method where a single interferometer (Follower) is employed and the masks (otherwise generated optically) are delivered electrically using an arbitrary waveform generator (AWG). In this way, the number of depths provided can be extended without the complexity of adding an interferometer for each depth needed, i.e., simply, by synthesizing the mask signal and using a mixer for each depth needed.

A comparison of operations in the two scenarios is presented, where the electrical signals generated by an AWG are either replicas of stored channeled spectra for different OPD values, similar to the LF protocol [3], or obtained from calculation of masks via an intermediate step of $g(k)$ and $h(k)$ calculation, i.e., according to the CLF protocol [4].

III. Data Acquisition

In order to perfect the replacement of the signal, otherwise provided by a Leader Interferometer (LI) with that synthesised electrically, a first intermediate step is to store photodetected

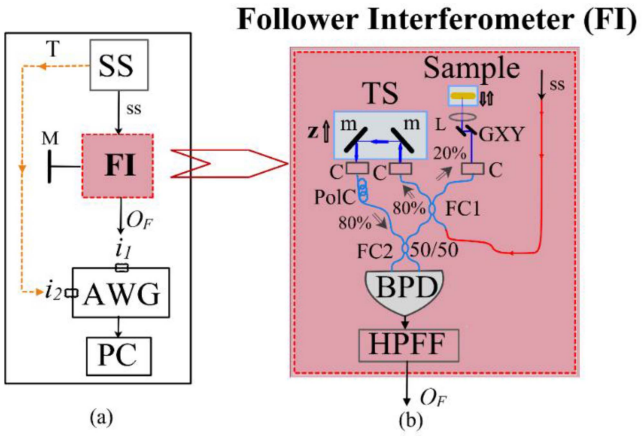

Fig. 1. (a) Schematic diagram used to store the photodetected signals, C(k), at the output O_F of the Follower interferometer (FI). SS: swept source; ss: optical signal, output of SS; M: mirror; AWG: arbitrary waveform generator; O_F: photodetected signal generated by FI; T: swept source electrical trigger. i_1, i_2: AWG inputs; PC: personal computer. (b) Schematic diagram of the FI. FC1, FC2: fiber couplers; C: collimators; m: mirrors, TS: computer controlled translation stage; L: lens; GXY: galvanometer scanning head; PolC: polarization controller; BPD: balanced photodetector; HPFF: high pass filter for the Follower interferometer.

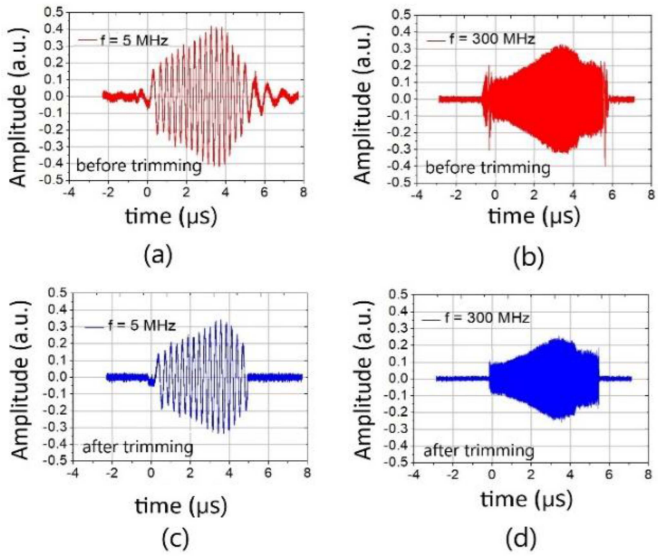

Fig. 2. Two photodetected signals, *C(k),* for two different optical path differences in the Follower interferometer (FI), at input i_1 of the AWG, before being trimmed by the AWG (a) and (b) and after being trimmed by the AWG before storage (c) and (d).

signals corresponding to channelled spectra from the OCT Interferometer (Follower). The diagram in Fig. 1 illustrates the setup that enables the acquisition of such signals. A swept source (SS), from Axsun Technologies, 1060 nm central wavelength, tuning at 100 kHz over a bandwidth of 111 nm (982-1093 nm) is used.

A mirror *M* is placed at different distances in the reference arm of the OCT interferometer and electrical versions of the channeled spectra, *C(k),* at the output O_F, are acquired and stored by the digital oscilloscope function of the AWG in Fig. 1. As AWG, a MokuPro from Liquid Instruments is used, with 4 input channels, under the control of a computer, PC. Here, input i_1 is used to receive photodetected signals. A second input, i_2 is always used for the trigger signal, T, from the SS.

When using more than one active inputs, the bandwidth is limited to 300 MHz. Moku is also equipped with 4 outputs to deliver different synthesized waveforms with maximum output frequency of 500 MHz (2 Vpp into 50 Ω). However, initial tests have shown inaccuracies in the shape synthesized over 300 MHz. Hence, in order to avoid sampling limitations, all signals generated by the AWG in the experiments described are limited to 300 MHz (in fact this is comparable with the bandwidth enabled by the clock of an Axsun swept source at 100 kHz).

In what follows, the AWG is used as storage of photodetected signals representing the channeled spectra and masks as well as for synthesizing mask signals in the form of real part of masks $M_z(k)$ in (3), to be applied to the LO input of the I&Q mixer. The signals are delivered in synchronism with the trigger *T*, applied to the i_2 input of the AWG.

The FI, in Fig. 1(b) is assembled around two directional couplers [3], light is split into a sample arm and into a reference arm using a 20/80 coupler, FC1, and the two waves from the reference and sample arms are combined in a 50:50, FC2 fibre coupler. In the object arm of the FI, a dual galvanometer scanning head (GXY, Cambridge Technology 6210 Series Galvanometer Scanners) is used to scan the optical beam over the sample. For the first sections on characterization and calibration, no lateral scanning is performed. The scanners will only be used in the section on imaging by the end of the paper. The output of the interferometer is fed to a balanced photodetector, BPD (Thorlabs, Model PDB481C, AC 30 kHz −1 GHz). A high pass filter, HPFF, with a cut-off frequency of 6.7 MHz (EF513 – Thorlabs) is used at the output to eliminate the DC and the low frequency variations of the photo-detected signals due to power variation during sweeping. OPD $= 2z$ adjustment in the FI is performed via a translation stage, TS, moved by z, controlled by a micrometer motorized stage VPX52 and a Newport driver, MM4006, that adjusts the length of the reference arm.

For calibration, a mirror, M, is used as a sample in the FI. As shown in Fig. 2(a) and (b) there are slow oscillating parts in the channeled spectra towards the edges of the tuning interval. Interference signal from the FI is cropped in similar ways to the procedure using a digitizer in conventional signal processing of swept source OCT signals, to obtain the spectra shown in Fig. 2(c) and (d), where the extreme chirps in the signal by the sweep edges are eliminated.

A. *Complex Leader Follower (CLF) Method*

The paper investigates comparatively different downconversion methods. Their performance in respect to axial range and axial resolution is assessed in comparison with the CLF method. In a previous report [10] it has been shown that this method leads to similar performance as achieved with the conventional SSOCT procedure of resampling followed by a FT [7]. An evaluation of timing required by the two methods, FT based and CLF depending on the number of sampling points was presented

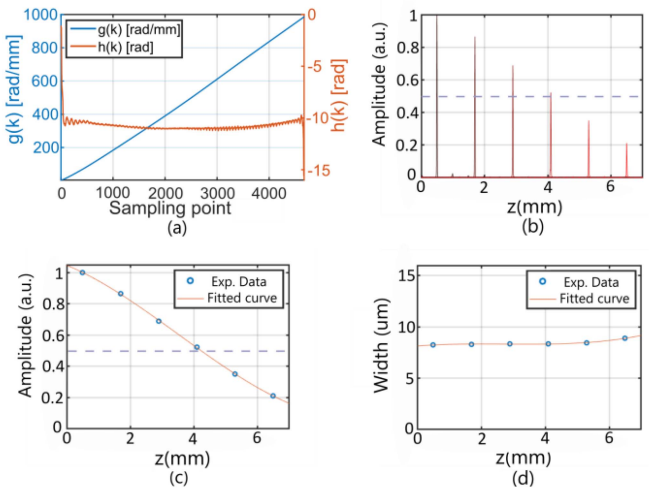

Fig. 3. (a) Calculated calibration functions *g(k)* and *h(k)* for the FI; (b) Roll-off produced with CLF; (c) Decay of A-scan peaks versus z in (b) and their FWHM versus z in (d).

in [13]. As explained in numerous previous reports, several *C(k)* signals are acquired for known steps in OPD. They are then used to calculate the two functions, *g(k)* and *h(k)* [4], [10], [13]. These functions are then used to generate masks, i.e., top hat of similar modulation to channeled spectra otherwise acquired experimentally [3] for a set of OPDs of interest. As there are two unknowns, *g(k)* and *h(k),* two C(k) acquisitions at least would be needed to form a system of two equations with two unknowns [4], [10], [13]. A few more allow some average over the errors of measurement hence 6 such *C(k)* are acquired and employed to obtain the *g(k)* and *h(k)* curves shown in Fig. 3(a). Using them, applying the complex LF protocol, the A-scan peaks for several OPD $= 2z$ values are calculated, as shown in Fig. 3(b). The decay of sensitivity with z in Fig. 3(b) and in Fig. 3(c) shows that at 50%, $Z_{0.5} \sim 4$ mm.

The graph of axial resolution variation versus z in Fig. 3(d) shows that the axial resolution is almost constant with a small increase at large z values. The values are in agreement with theory. If resampling is applied as described in [7], [10] and applying FT to data, similar results are obtained. However, as a known fact with micro-electro-mechanical system (MEMS) tunable sources, the profile of tuning varies with time. Therefore, from the moment the channeled spectra are acquired and *g(k)* and *h(k)* functions calculated, until they are used, the function *g(k)* varies. This leads to quicker decay with z and some deterioration of the axial resolution. In the signal processing practice, either using resampled data and fast Fourier Transform (FFT) [7] or the protocol of complex LF (CLF) [4], [10], [13], a clock is used to keep track of these variations, in which case consistent results are obtained over time, with tolerance to *g(k)* variations over time.

Using $\Delta\lambda = 100$ nm in the equation below:

$$\delta z = 0.6 \cdot \frac{\lambda^2}{\Delta\lambda} \tag{5}$$

where the 0.6 coefficient is employed for a top hat spectral profile [14] suggests an axial FWHM resolution of 6.7 μm. Obtaining A-scan peaks with a FWHM resolution close to the expected theoretical resolution in Fig. 3(b) and (d) validates the signal processing procedure, either using conventional FFT after resampling or the CLF procedure. The decay of amplitude with depth is another parameter, if FFT is calculated from non resampled data, the decay with OPD would be much faster. The axial range should in fact be commensurate to the dynamic coherence length of the swept source, according to:

$$Z_{0.5} = 0.25 \cdot \frac{\lambda^2}{\delta\lambda} \tag{6}$$

where $\delta\lambda$ is the dynamic linewidth of the swept source. The chirp due to nonlinearities in tuning described by *g(k)* and dispersion in the interferometer described by *h(k)* reduce the axial range if FFT is applied to non resampled data. The same happens in the practice of CLF if incorrect profiles for functions *g(k)* and *h(k)* are obtained.

These two parameters, axial resolution and decay of strength with OPD will be measured for several versions of the different downconversion configurations implemented here. The paper evaluates comparatively the performance of downconversion in terms of axial resolution and decay with OPD using an AWG instead of using a Leader interferometer and such performance will also be related to the values obtained with CLF in Fig. 3(c) and (d).

To illustrate the versatility of AWG for DLF, several measurements of the coherence gate profile characterizing the DLF operation are performed. Main application of the AWG would be to act in a DLF pair with an OCT interferometer (as FI). The results will be labelled as "EO", i.e., electrical – optical in comparison to the case "OO" (optical – optical) used in previous reports, using two interferometers [5] and three interferometers [6]. We will compare the axial range Δz and the axial resolution δz such obtained with sets of measurements of the DLF scheme in either OO or EO cases. 6 electrical signals are collected for 6 channeled spectra acquired for different z values adjusted by the translation stage, TS, in the FI, where OPD $= 2z$. The parameter z was varied in steps of 1.25 mm, corresponding to a jump in RF frequency of the channeled spectrum signal measured by a RF analyzer of 50 MHz. As the spectrum is chirped, covering a band of RF frequencies, for each OPD value, the maximum frequency in the RF spectrum is retained only.

B. From Optical Generation to Electrical Generation of the Masks

Fig. 4 illustrates the two cases investigated, OO (optical - optical) and EO (electrical - optical) where in both cases, the DLF multiplication of signals in (4) is performed using an *I&Q* mixer, X (Analog Devices, LTC5584, 30 MHz to 1.4 GHz), similar to that employed in [6]. A third experiment, EE (electrical - electrical) is also shown, valuable for testing the operation of the *I&Q* mixer.

OO, refers to the original DLF procedure [3], [5] using two interferometers, fed by the same swept source. In the OO case, the second interferometer, as LI, is similar in components to the FI [5], [6] shown in Fig. 1(b), the only difference is that

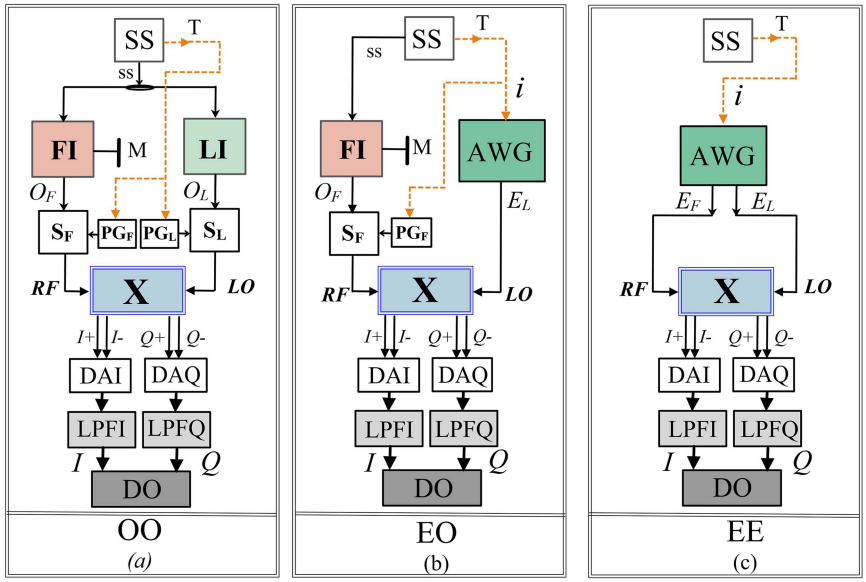

Fig. 4. (a) Optical – optical (OO) case, multiplication of photodetected signals at the output of two interferometers, where the mask is obtained optically; (b) The new DLF method, Electrical – Optical (EO) case, multiplication of signals, one generated electrically, the mask, stored/generated by the AWG and the other generated optically; (c) Electrical – electrical (EE) case, multiplication of electrical signals for operation validation of the mixer X. SS: swept source; ss: optical signal, output from the SS; FI: Follower interferometer; LI: Leader interferometer; PG_L and PG_F: pulse generators: S_F, S_L: switches; AWG: arbitrary waveform generator; O_F, O_L: photodetected signals generated by the FI and respectively by the LI; T: electrical trigger; *i*: AWG input; E_F, E_L : electrical signals as masks, at the outputs of the AWG; X: *I&Q* mixer; *RF*: X signal input; *LO*: X local oscillator input; *I*+, *I*-, *Q*+, *Q*-: outputs of the X mixer; DAI: differential amplifier for the *I* signal; DAQ: differential amplifier for the *Q* signal; LPFI: low pass filter for the *I* signal; LPFQ: low pass filter for the *Q* signal; DO: digital oscilloscope.

it does not have a galvanometer scanner. In this case, the two channeled spectra from the two interferometers are trimmed by using switches, S_F and S_L under control of pulse generators PG_L and PG_F controlling the timing of the waveforms, in terms of their length and delay in respect to the swept source trigger, T. Mini circuits ZASWA-2-50DRA+ are employed as switches and Hewlett Packard HP8112 A, 50 MHz as pulse generators. The switches allow selection of the most useful parts of the sweeps to be used to create the images, similar to trimming performed by a digitizer in conventional swept source OCT and similar to trimming performed here by the AWG itself before storage of signals, as shown in Fig. 2. In this way, edge pulses of the sweeps, with extreme chirps are eliminated, improving the mixing operation. The Axsun swept source emits for each $\sim$ 6 μs of the 10 μs interval, hence the gated interval selected, is $\sim$ 5.5 μs.

EO stands for the new method, it signifies a DLF procedure where the local oscillator (LO) input of the *I&Q* mixer is fed not by the photodetector in a LI, but by the AWG. EE corresponds to the case where both inputs of the *I&Q* mixer X are fed by signals synthesized by the AWG. Essential for the downconversion is to provide copies of channeled spectra in synchronism with the real time provision delivered by the FI. Therefore, before being sent to the mixer inputs, the two channeled spectra, *C(k)* from the interferometers and from the AWG are checked on a 10GSa/s digital oscilloscope and cable delays are employed to secure synchronism with an error less than 1 ns when using the OO method and digital delay on the AWG when using the EO method.

As shown in Fig. 4, a differential amplifier, DAI, is used to produce the difference of the two *I* outputs of the *I&Q* mixer, X, and another differential amplifier, DAQ, for the difference of the two *Q* outputs of the mixer:

$$I = I_+ - I_- \text{ and } Q = Q_+ - Q_- \tag{7}$$

The signals *I* and *Q* are low pass filtered by respective LPFI and LPFQ to obtain I_{LPF} and Q_{LPF}. The difference preparation, amplification and low pass filtering is achieved by two Stanford Research low noise amplifiers SR560 (LNA)s. The I_{LPF} and Q_{LPF} at the outputs of the two LPFI and LPFQ are connected to the two inputs of the digital oscilloscope, DO, to evaluate the DLF output, according to (4) via:

$$\mathrm{X\,(k)} = \mathrm{Area}\{\sqrt{I_{LPF}^2 + Q_{LPF}^2}\} \tag{8}$$

where Area signifies the area covered by the shape of X(k) over bias zero on the DO screen, evaluated over a sweep period of 10 μs using the Math functions menu of the DO.

IV. Experimental Results

Three sets of results in respect to calculation of (4) using the *I&Q* mixer are presented, with signal from the FI applied to the RF input of the X mixer:

a) OO downconversion, where the photodetected signal from the LI is applied to the LO input of the mixer (Fig. 4(a));
b) EO downconversion, where electrical signal delivered from the AWG is a stored photodetected signal that is applied to the LO input of the mixer, to perform the LF protocol [3] (Fig. 4(b)).

For the generation of masks, the following steps are performed:

i) Acquisition of photodetected signals corresponding to channeled spectra for different OPD values: A total of 6 such signals are stored in steps of 1.25 mm, starting from $\sim$ 20 MHz corresponding to a step of 50 MHz as measured by a RF spectrum analyser.
ii) After the photodetected signals are loaded, they are cropped (as shown in Fig. 2) to eliminate their end tails.
iii) EO *g&h* downconversion, where *g(k)* and *h(k)* functions are evaluated that allow calculation of masks at any desired OPD values and where the electrical signal from the AWG is that of a mask so calculated to perform CLF protocol [4] (Fig. 1(b)).

For the generation of masks, the following steps are performed:

i) Acquisition of photodetected signals corresponding to channeled spectra for different OPD values: A total of 6 such signals are stored in steps of 1.25 mm, starting from $\sim$ 20 MHz corresponding to a step of 50 MHz as measured by a RF spectrum analyzer.
ii) *Calculate the functions g(k) and h(k):* a Matlab script is written that implements the steps described in [4], [10]. The program needs the following parameters: OPD interval between the OPD values used for acquisition of channeled spectra (mm), starting and finishing positions (mm) and the number of points. Calculation is quick, subsecond. After the photodetected signals are loaded, they are cropped (as shown in Fig. 2) to eliminate their end tails and after that a file with *g&h* functions is computed;
iii) *Mask generation:* in order to generate masks, three input parameters are required: starting point (mm), step between the OPD values of the masks (mm) and the number of masks desired. CLF according to procedures described in [4], [10] produces complex masks and the square root of the summation of real part of the mask squared with the imaginary part of the mask squared is output here as a *g&h* mask for each k. This step takes a few seconds.
iv) *Transfer of masks to the output:* Final step implies the AWG function where amplitude and delay of the created mask in respect to the swept source trigger T is adjusted to maximize the X output signals. Under PC control, any mask so calculated for any desired depth is outputted to one of the AWG outputs connected to the LO input of the *I&Q* mixer.

A. Decay of Sensitivity With OPD

As explained above, experimental *C(k)* signals were stored for 6 OPD values determining 20, 70, 120, 170, 220, 270 MHz. The OPD/2 = z was changed using the computer controlled translation stage, TS in Fig. 1(b) altering the length of the reference path in the FI. The photodetected signals were trimmed as explained in Fig. 2, to be used as stored masks for EO as well as used to determine *g(k)* and *h(k)* for EO *g&h* case. Having the *g(k)* and *h(k)* functions, masks for the same *z* values were generated.

In Fig. 5, the decay with OPD is evaluated engaging the X mixer, by performing downconversion in the three cases of OO, EO and EO *g&h*. The higher frequency components generated by multiplication are attenuated by the low pass filters, LPFI and LPFQ that perform the average in (4). Hence the resolution of DLF is dependent on the LPFI and LPFQ bandwidth. The bandwidth of the downconverted signal is that of pulses at the swept source frequency, of pulsewidth $\sim 5\ \mu$s. Therefore, results are presented for three values of the low pass filter bandwidth, of 1 MHz, 300 kHz and 100 kHz. The FI output is connected to the RF input of the mixer X and either the LI output in the OO case or electrical signals from the AWG are applied to the LO input of the mixer. For the OO case, the mixer produces the product of the FI output and LI output, respectively of trimmed signals O_F and O_L in Fig. 4. For the EO case, the mixer produces the product of the FI output with the stored photodetected signal corresponding to different modulation in the channeled spectra, for different OPD values in the FI. For the EO *g&h*, the analog product of the FI output and calculated masks via the CLF protocol is evaluated.

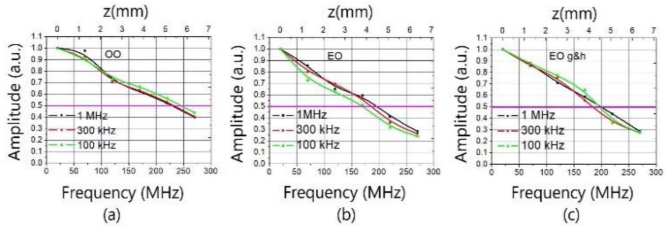

Fig. 5. Decay of sensitivity with OPD for three different scenarios (a) OO, (b) EO, and (c) EO *g&h*. All of them were obtained using the *I&Q* mixer and LPFs for 1 MHz (black), 300 kHz (red) and 100 kHz (green).

The mixer X was tested and presents no significant variation of amplitude at its output in the range 20 MHz to 1.4 GHz. For the OO case, the amplitude of the X signal calculated using (8) reduces to half close to 5 mm, while for the EO and EO *g&h* by 4 mm. These values should be compared with 4 mm in Fig. 3(b) and (c) for the CLF. The CLF results in Fig. 3(b) and (d) involve digitization while OO employs photodetection and analog mixing only.

As already presented [5], longer axial range was obtained via OO downconversion in comparison with the CLF using digitization, where downconversion can reach the axial range limited by the coherence length of the SS, that is here larger than the limit imposed by the digitizer sampling rate. In addition, the OO case presents tolerance to *g(k)* variation in time, similar to that of using a clock in the conventional SSOCT signal processing. Both EO cases, as well as the CLF case suffer from *g(k)* profile variations from the time either the channeled spectra were stored or calculated until they are used. The effect of such changes in time was already documented in Fig. 6 in [5] and in the Fig. 4 in [15]. In the OO case, both interferometers are driven by the same SS, hence the same *g(k)* function affects the chirp of the two signals averaged in (4). In the CLF case in Fig. 3(b) and (c) and all EO cases, the two signals in the product (4) may correspond to different *g(k)* functions, due to the time lapsed from the moment of spectra acquisition to the moment of mask utilization. This may explain the lower value of axial range of the CLF and EO cases in comparison with the OO case as already commented above.

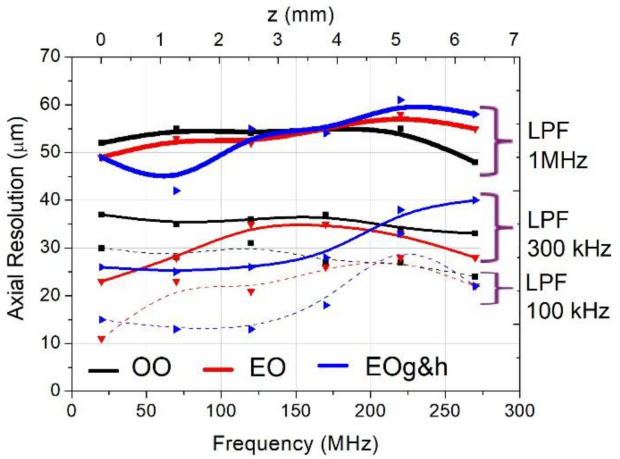

Fig. 6. Axial resolution versus z using the *I&Q* mixer and LPF on 1 MHz, 300kHz and 100 kHz, 12 dB.

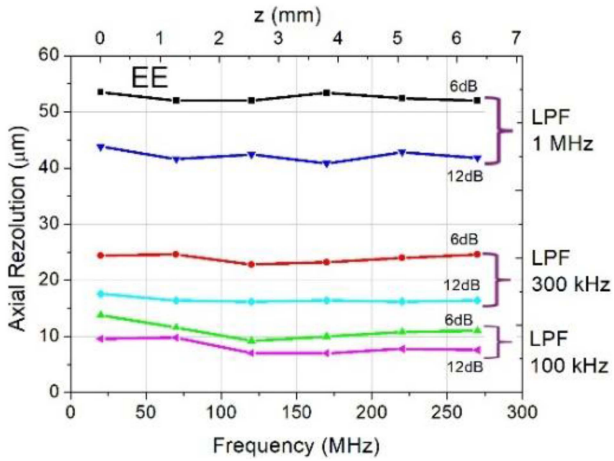

Fig. 7. EE case, axial resolution versus the LPF cut-off frequency using masks synthesised by the AWG, for two slopes of attenuation of the LPFI and LPFQ.

A decay graph for the EE case is not produced, as this would have implied applying the same mask to the two mixer inputs. As all masks are generated as top hat, they have the same amplitude, while in OO and EO case, the amplitude of the signal from the FI varies with OPD. It can be noticed from the graphs in Fig. 5 that the low pass filter bandwidth has no significant effect on the OO DLF and EO DLF variation with OPD. As far as the axial range is concerned, the results in Fig. 5 demonstrate successful replacement of the optical generation of masks with electrical generation, respectively of the LI with an AWG.

B. Axial Resolution Versus OPD

Experimental channeled spectra *C(k)* were stored for 6 OPDs values determining 20, 70, 120, 170, 220 and 270 MHz. The OPD/2 $= z$ was changed using the PC controlled translation stage, TS in Fig. 1(b), altering the length of the reference path in the FI. Having the *g(k)* and *h(k)*, masks for the whole range of z up to 6.3 mm were generated in steps of 2 μm according to the protocol described in [4]. The axial resolution is evaluated by using the translation stage to vary the distance z around that corresponding to each of the channeled spectrum frequency above. The amplitude of the (4) based on the product obtained between C(k) and the mask versus z represents an equivalent "A-scan peak" (not shown). The width of such a profile versus z represents the axial resolution of the method and represented graphically in Fig. 6.

Three cases are considered for all three experiments in Fig. 6, using low pass filters LPFI and LPFQ of 1 MHz, 300 kHz and of 100 kHz. For the OO, the axial resolution is between 45–55 μm at 1 MHz, between 30–36 μm at 300 kHz, and improves to 20-30 μm at 100 kHz. For the EO cases, the axial resolution is between 48–58 μm at 1 MHz, between 23-36 μm at 300 kHz, and improves to 10-24 μm at 100 kHz.

To disentangle the LPF bandwidth from the *g(k)* and *h(k)* variations, an EE experiment is implemented. In this case the axial resolution is evaluated by using two masks synthesized at two outputs of the AWG, a central mask corresponding to the frequency in the set above sent to the RF input of the mixer and by sending signal of a different mask to the LO input of the X mixer, where the mask index is varied in steps of 2 μm, between minus 20 μm to plus 20 μm around the index of the central mask. Measurements were performed for two slopes of LPF attenuation available on the Stanford Research LNA SR560, 6 dB and 12 dB, in Fig. 7. Such measurements illustrate the mixer performance irrespective of precision in obtaining the *g(k)* and *h(k)*. Masks obtained via *g&h*, CLF protocol, i.e., all obtained under the same *g(k)* and *h(k)* conditions, are applied to the two inputs of the X mixer, for several values of the LPF cut-off. The amplitude of the product obtained versus the mask index represents an equivalent "A-scan peak" that given the increment in OPD between the indices of the masks used, can be represented along the OPD axis. The width of such a profile versus frequency of the mask applied to the LO input is in fact the axial resolution of the method using the mixer, as represented in Fig. 7. As shown, an expected axial resolution $\sim$ 10 μm can be obtained with a low frequency cut-off 100 kHz and using a 12 dB decay. For point measurements this can be lowered further, but for imaging at 100 kHz sweep rate, this is already comparable with what would be a minimum bandwidth when sweeping at 100 kHz, lower values would smear the lateral pixels in the image. The effect of the low pass filter bandwidth will be further assessed on the aspect of an *en-face* image of a tilted mirror below.

As far as the axial resolution is concerned, the results in Figs. 6 and 7 demonstrate successful replacement of the optical generation of masks with electrical generation, respectively of the LI with an AWG. EO can operate as well as OO as long as the tuning nonlinearity curve, *g(k)*, does not vary in time. Here we used a swept source known to exhibit *g(k)* variations in time [5], [15] that may explain slightly worse axial resolution in the EO case in comparison to the OO case. Also, an important observation is that while for the axial range, as shown by graphs in Fig. 5, the low pass filter cut off is not that important, in order to achieve good axial resolution, as suggested by Figs. 6 and 7,

an abrupt decay slope is essential together with a low value for the cut off.

C. Sensitivity Measurements

Sensitivity measurements are performed in all cases, OO and the two EO cases. When performing sensitivity measurements, a RF amplifier Mini-Circuit ZFL-1000-VH2+, 0.1 – 1 GHz, 18 dB, is used to amplify the output signal O_F, after the HPFF. A small signal was applied on the X-scanner to scan the beam of 1 mW over a mirror oriented perpendicularly on the optical axis.

An attenuation was introduced in the sampled arm, to reduce the interference signal by a factor, a, larger than 1000. Then signal to noise ratio (S/N) was measured by performing the ratio between the signal obtained on the scope calculating (8) over the noise left in the system when the sample arm was blocked and still calculated with (8). Sensitivity was then evaluated as the product of a with the S/N and the result subject to 20 log calculation. The CLF performed in the FI lead to over 85 dB. In all downconversion cases however, OO, EO with stored spectra and EO *g&h*, similar values are obtained, of 70–74 dB, in line with such previous measurements [5], [6].There is also reserve in obtaining better S/N ratio by eliminating the fibre coupler from the SS that divides power to the FI and LI. For the EO DLF, such coupler can be eliminated and the Follower interferometer will receive larger power and so, better S/N becomes achievable. On the other hand, downconversion manifests more noise, due to mixing products and operation around zero Hertz, where 1/f noise is large. However, the EO method is superior to OO method at OPD values where there are deterministic RF components in the photodetected signal due to stray reflections in the interferometer or coming from the swept source (measured with the object arm blocked). The masks synthesized by the AWG do not incorporate such oscillations, hence the EO case should perform better than the OO case in the spectral range in the vicinity of deterministic oscillations.

D. Comparison of OO and EO Images

As a final validation for replacing interferometers with AWGs, in delivering the Leader signal, *en-face* OCT images are collected in the case of EO *g&h* with calculated masks from *g(k)* and *h(k)*. Signal from either *I* or *Q* is sent to an imaging device controlled by triggers for line rate and frame rate controlled by drivers for the two galvanometer scanners using the same *en-face* display system on two channels as reported in [6]. *En-face* OCT images are obtained using the DLF protocol from objects placed at 3 cm away from an achromat lens, L of 3 cm focal length at 3 cm from the galvanometer scanning head in Fig. 1(b). This determines a lateral resolution in the focus better than 20 microns and a Rayleigh range of 1 mm.

The fast galvanometer scanner (line), X, is driven by a triangular signal of 2 ms period while the slow galvanometer scanner (frame), Y, is driven by a sawtooth with a period of 0.5 s. An *en-face* image is generated every 0.5 s with 500 interleaved lines, each line made of 100 lateral pixels, alternating from a line corresponding to scanning left to right, to the next line corresponding to lateral scanning for right to left. Voltage

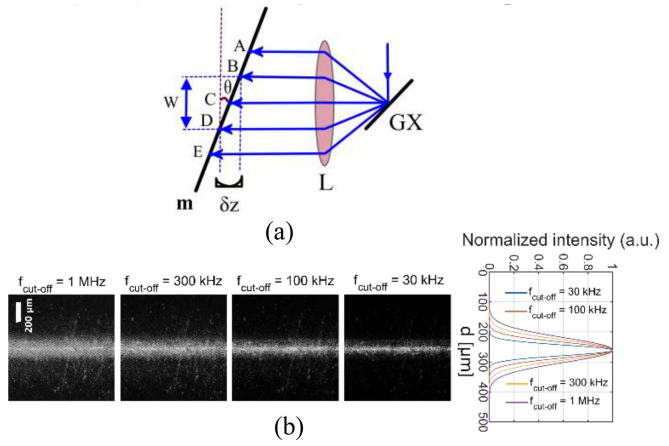

Fig. 8. (a) Fan of rays from the galvanometer scanner covering the tilted mirror from A to E. However only the part of the mirror between BD is sampled by the *en-face* OCT image, corresponding to a difference in depth between B and D determined by the axial resolution; (b) Effect of the LPF cut-off frequency on the aspect of the *en-face* OCT images of a tilted mirror in the vertical plane. Vertical and horizontal size in the OCT *en-face* images: 1 mm × 1 mm; The profile on the right represents an average over the 100 columns in the images on the left.

applied to the two lateral scanners determine a lateral image size of 2.1 mm.

An equivalent procedure for measuring the axial resolution, which was found easier to implement and with immediate illustration of the axial profile, and more stability than point by point measurement along depth, is described below. To this goal, in a first set of experiments, the object considered is a mirror whose normal is tilted at $\theta \sim 20°$ from the optical axis shown in Fig. 8(a). The intersection of the coherence gate with the tilted surface leads to a bright patch in the image. The width of the patch, W, gives a direct view of the width of the coherence gate, δz:

$$\delta z = W \cdot \tan\theta \tag{9}$$

The effect of the low pass filtering is evaluated in Fig. 8(b) on 4 *en-face* OCT images collected using a mask corresponding to the largest OPD evaluated here corresponding to 270 MHz, applied to the LO input obtained via the *g&h* protocol, i.e., images are presented for the EO *g&h* case. The larger the OPD, the wider the A-scan peak becomes if resampling is not right when using the FT based OCT, or when using incorrect shapes for the *g(k)* and *h(k)* functions when performing the LF protocol or the CLF, i.e., manifestations of incorrect calibration are easier seen when the OPD is large. The two LPFs are set to 1MHz, 300 kHz, 100 kHz and 30 kHz and slope at 12 dB. By averaging over all columns in each *en-face* OCT images, the profiles shown in Fig. 5 right shows a FWHM of W improvement from 69 μm at 1 MHz to about 32 μm at 30 kHz, giving δz respectively of 25 μm and 11 μm. The advantage of such measurements is two fold: (i) providing a real time evaluation of the axial resolution and (ii) securing average over several realizations (lateral scan lines). The dust or scratches on the mirror may disturb slightly the results of such estimation. The images show that in order to comply with the imaging bandwidth, determined

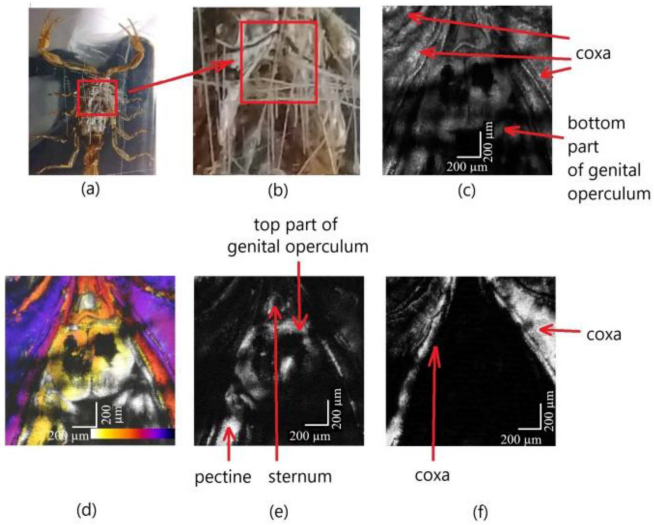

Fig. 9. Images obtained from a Manchurian type scorpion using 330 masks calculated via complex LF and delivered by the AWG to the LO input of the X mixer (a) Photo of the scorpion embedded in a transparent plastic block; (b) red square shows the area imaged in the next images (2 mm × 2 mm), displaying scratches made on the top surface of the transparent plastic block; (c) Intensity summation over all 330 *en-face* OCT images obtained using all 330 masks [See Supplementary Information Video 1].); (d) color-coded representation of images versus z of masks used from z = 3.5 mm (150 MHz), white, to z = 4.82 mm (205 MHz), blue purple (measured in air); (e) *En-face* OCT image at z = 3.81 mm (163 MHz); (f) *En-face* OCT image at z = 4.45 mm (190 MHz, white is at the top of the sample while blue purple is inside the sample.

by the sweeping rate, a compromise between axial resolution and smearing of features in the *en-face* views is needed.

In fact, this imaging procedure, of a tilted mirror, was also found helpful in adjusting the delay with which the AWG delivers the mask to the mixer. In practice, the delay adjustment using the tilted mirror, was more effective than that using the digital scope to assess the delays between the two waves, coming from the FI and from the AWG. The AWG has the possibility to digitally delay the output waveform in steps of fractions of the period controlled by the trigger. Looking at an image as such displayed in Fig. 8, the delay was adjusted to secure a minimum for the thickness W of the bright patch. If minimization of thickness of the bright patch is sought in the process, and not an exact evaluation of the axial resolution, then the mirror can be left at any angle, with the bright patch resulting at any angle in the plane of the image. Otherwise, producing a patch oriented exactly horizontal or exactly vertical is time consuming.

A second object imaged is a Manchurian type scorpion [16], [17] embedded in a transparent plastic block, as shown in Fig. 9(a). The optical power on the sample was 2 mW, so an amplifier from Minicircuits, 0.1 – 1 GHz, 18 dB was added to amplify the signal O_F at the FI output before being sent to the switch S_F in Fig. 4. The block with the scorpion was positioned and imaged with the stomach facing the lens, L, in Fig. 1(b). A volume of data is acquired, by capturing 330 frames at 4 μm interval using 330 synthetized masks. Given the large height of the polymer block incorporating the scorpion, the OPD = 0 in the OCT interferometer (FI) is placed inside the polymer behind the scorpion. Masks were obtained via the CLF protocol using *g(k)* and *h(k)*, separated by 4 μm. Fig. 9(b) illustrates a selected part in the square that is imaged in the other 4 images. In Fig. 9(c), the *en-face* image shows a superposition of all images obtained by using all 330 masks. This is equivalent to the image in the common practice of SSOCT where the photodetected spectrum is deprived of the DC and the remaining modulation is rectified to obtain an overall *en-face* image to guide the investigation. A color depth coded *en-face* image is presented in Fig. 9(d) where the z values of each of the 330 masks correspond to a specific color. The other two images display thin *en-face* OCT slices obtained by using the masks for 3.8 mm at 163 MHz in (e) and for 4.45 mm at 190 MHz in (f). Identification of features seen inside the scorpion are based on [16], [17], [18].

The horizontal black lines in the images correspond to accidental scratches on the top surface of the transparent plastic block casting shadows in the volume of images underneath.

By changing the mask from the set of 330 masks, EO DLF *en-face* images have been generated and then used to produce the volume shown in the Supplementary file Video 1. The masks covered a spatial interval from z = 3.5 mm to 4.82 mm (measured in air) corresponding to a frequency interval of 150 – 205 MHz. For the imaging, the focus of lens L was positioned inside the sample, where frequency ∼ 180 MHz. The time taken in the two EO cases to change the mask with the next in the set is 1-2 seconds, followed by imaging, another second and saving a few more seconds. Hence time to generate the video is longer than 10 minutes and depends on the number of frames used. Although this time can be improved by automatizing the process, this is not a recommended regime of operation for the DLF. The video was only produced to demonstrate similar quality of volume generated by using EO DLF to that obtainable via OO DLF [6]. The recommended regime is that of serving the 6 potential applications described in Section IV below.

The DLF is not proposed here as a modality to replace the current FT based OCT or the equivalent CLF method using commercial swept sources at hundreds of kHz delivering a whole volume over many more depths quicker (in a few seconds, depending on the number of lateral pixels and sweeping speed). DLF can prove useful as an add-on to any A-scan based OCT system (FT based OCT) or to any CLF based OCT, adding capability of fast display of a single or of a few *en-face* slices. A DLF add-on may also find use in ultra fast SSOCT or SSOCT systems using a swept source with a long coherence length. More in respect to utility of DLF is presented in the next section.

A different view is presented in Fig. 10, where B-scans in (b) and (c) are associated to the C-scan whose depth can be scrolled through the volume of the video [See Supplementary file Video 1]. Some streaks in the (b) and (c) images are seen as tails in depth due to secondary lobes in the axial resolution profile, due to the large bandwidth of the LPF used, of 1 MHz. With the LPF on 100 kHz, the streaks in depth are reduced but the lateral resolution suffers.

The AWG has 4 outputs and in principle, 4 slices for 4 depths can be displayed simultaneously. We had at our disposal components for two images only, hence two simultaneously acquired and displayed images only are shown in Fig. 11. The AWG outputs two masks at two of its outputs and then via two

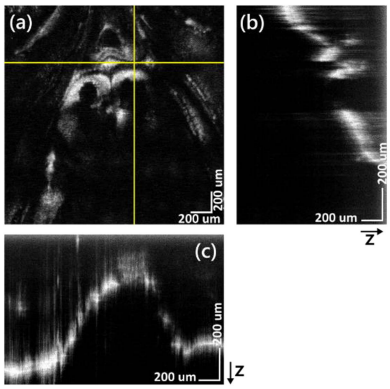

Fig. 10. Orthogonal slicing through the spider, with the depth of the *en-face* image at 3.81 mm (measured in air) (163 MHz) inside the transparent plastic block within which the scorpion is embedded in. Images size: a) 2 mm × 2 mm, b) 1.32 mm in depth measured in air x 2 mm c) 2 mm × 1.32 mm measured in air. All scale bars are 200 μm.

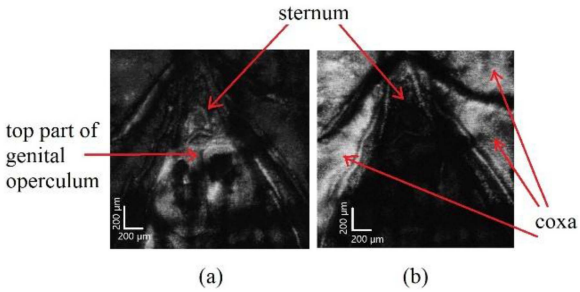

Fig. 11. Two *en-face* OCT images from two different depths simultaneously displayed, using EO regime of operation and masks from the set of 330 obtained via the CLF protocol. (a) z = 3.31 mm (f = 142 MHz); (b) z = 4.175 mm (f = 178 MHz). Image size 2 mm × 2 mm.

similar active *I&Q* mixers, two *en-face* images are displayed from the scorpion from different depths, as selected by the two masks. Any two masks from the set of 330 masks used for the experiment above could be used for simultaneous display of two *en-face* OCT images from different depths.

Another set of images were obtained from the Manchurian type scorpion in a separate experiment where the focus was positioned inside the sample at ∼ 75 MHz and *en-face* images were collected in both OO and EO regimes of operation (Fig. 12). The OO images produced are similar to those already presented in [6], hence here for comparison of the OO and OE regimes, only two pairs of images are shown.

V. Potential Applications of the New EO DLF OCT Method

Using an electrically generated Leader signal for downconversion instead of the optical signal delivered by an interferometer as reported so far [5], [6] opens avenues for more compact and much simpler assembly of OCT instruments. As demonstrated, the electrical signal can be delivered by an AWG. This can output a stored version of the photodetected signal of the same interferometer for a selected OPD value when the object is replaced by a mirror. The AWG can also be employed to synthesize electrical versions of photodetected signals at the interferometer

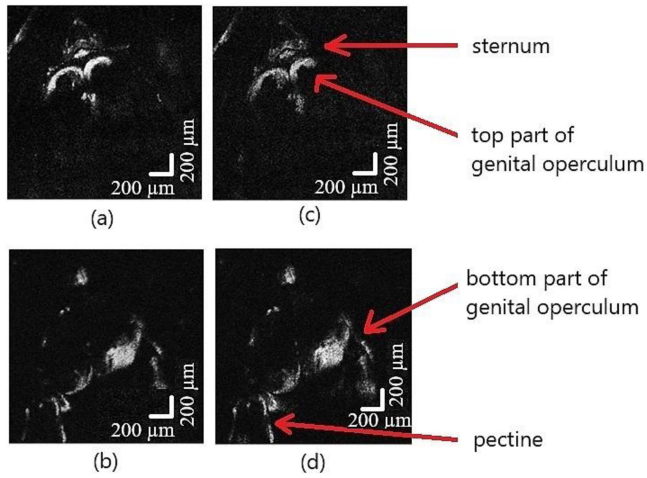

Fig. 12. Comparison of OO regime of operation (a) and (b) versus EO (c) and (d) for two *en-face* OCT images from two different depths at f = 70 MHz (top row images) and f = 88 MHz (bottom row images) [focus was positioned inside the sample at ∼ 75 MHz] Image size 2 mm × 2 mm.

output according to the CLF protocol, based on measurement of the functions *g(k)* and *h(k)*. Such generated signals act as synthesized masks otherwise used in CLF OCT [4], [10], [13] employing a high-speed digitizer. By selecting the mask from a set of masks, the OPD of the *en-face* section can be changed and in this way, *en-face* images from different depths can be produced. In comparison with the procedure in the original paper on the LF principle [3] and in the DLF reports [5], [6] where the OPD in the LI dictates the depth from the object placed in the FI, here the depth in the object is dictated by changing the mask synthesized. However, changing the mask in the OO case is mechanical (modifying the OPD in the MI, by moving a mirror or modifying a distance between fibre ends in the reference path of the MI), while in the EO case is electrical. Electrical synthesis is more elegant and easier, with net advantage in terms of time if masks at large difference values in their OPDs are to be swopped. In addition, for defined shapes of masks, simpler low-cost electronic solutions are possible when only a few specific signals are needed and that would be the goal of a further study.

In addition to the functionality described in Figs. 8 –10, where EO DLF proved equal in performance to OO DLF, 6 more potential applications are envisaged:

1) *Add on en-face functionality to a conventional SSOCT system:* Using two AWG outputs, comparison of *en-face* views from different depths can be performed by EO DLF as already demonstrated using DLF OO in Ref [6], by varying the OPD in the LI. Instead here selection in depth is executed non mechanically by varying the index of masks as shown in Fig. 11. This functionality can be added to any conventional SSOCT system by tapping into the photodetected signal delivered by the balanced photodetector and by tapping into the trigger signal from the swept source. In this way, real time *en-face* views can be presented in parallel with high resolution detailed cross

TABLE I
COMPARISON OF THE CONVENTIONAL FFT BASED OCT WITH DIFFERENT LF OCT MODALITIES

	Conventional FFT + data resampling	LF	CLF	OO DLF	EO DLF
Number of photodetectors for N depths	1	1	1	N+1	1
Mask production	NA Mask is the monochromatic factor in the FFT basis calculation	Experimental, using the same FI	Calculated from g(k) and h(k) obtained by acquiring at least two spectra using a mirror in the FI	Experimental, using 1 to N LIs	Synthesised electrically
Multiplication of the mask with the photodetected signal from the FI as per eq. (4)	Digital	Digital	Digital	Analogue	Analogue
Axial range limited by	Digitiser sampling rate			Optical source coherence length	
Potential for parallel processing	Limited			Via optical integration of LIs with photodetectors and mixers	Via electrical integration of AWGs and of mixers
Real time production of *en-face* OCT images using > 10 MHz rate swept source or large coherence length swept source	While acquisition is fast, the use of a digital oscilloscope delays the time of image delivery			Possible	

section imaging or volume imaging, for guidance of detailed cross section imaging. This can be achieved without increasing the computation load, as the multiplication of mask with the photodetection signal is performed by the analogue mixer. Tapping into electrical signals should not impact the signal to noise ratio if electronic amplifiers are employed with proper impedance matching.

2) *Real time, high resolution en-face display complementing FFT based conventional B-scanning:* A DLF generated *en-face* image is thin, i.e., it exhibits the axial resolution of the OCT, of a few microns. This may provide more hints on location, tilt and orientation of sample in front of the scanning head than the simple display of a projected *en-face* image from all depths that is conventionally displayed in SSOCT by summing all spectral modulation of the channeled spectrum. In conventional FFT based OCT, a volume of A-scans is collected and then cross sections (B-scans) are sliced from positions in a static *en-face* image. This is a cumulated, static *en-face* image over all depths, and is used as guidance. Having a thinner *en-face* view may provide more diagnostic power when combined with the detailed cross sectioning. Not only better resolution than the static *en-face* image used now, but the *en-face* image can be generated in real time, at higher speeds of volumetric data collection, using MHz sweep rate modern swept sources.

1) *Real time, en-face display for ultra fast swept sources or long coherence swept sources:* The DLF may find a niche application as an add on for FT based OCT or CLF based OCT, acting as a guide in positioning the sample imaged. When either the sweeping speed is large, exceeding tens of MHz [19], [20] or the coherence length of the laser exceeds several meters [21], sampling rates exceed tens of GHz, secured by employing digital scope digitisers only. For example, for cubic metre range OCT [21] where the sweeping rate was only 100 kHz, due to a coherence length of $\sim$ 200 m, the RF photodetected signal exceeded 10 GHz, hence a 50 GS/s digital oscilloscope was employed. Data is acquired fast, but production of images can only be performed after transfer of data from the digital oscilloscope. Therefore, a single B-scan exceeded one minute. For such experiments, a guiding image delivered by DLF can be useful to properly adjust the sample in front of the scanning head. We anticipate that for such cases, where images cannot be produced in real time, it would be useful to employ a guiding tool based on DLF. OO DLF requires a second fast photodetector in the LI and a low cost digitiser. EO DLF however does not need an extra interferometer hence no need of a second fast photodetector, but needs an AWG to generate the mask, that in case of MHz swept sources, should synthesise signals of tens of GHz. For such cases, lower cost AWG circuitry should be developed to generate chirped masks. An example in this respect is Ref [22], where the sweeping rate was only 200 kHz, but with a coherence length exceeding 10 cm, by the time of the experiment the lack of a high speed digitiser was compensated by performing OO DLF.

2) *Sparse investigation in depth:* With the recent trend in performing SSOCT at sweeping rates exceeding 10 MHz [19], [20], DLF can find applications where a whole A-scan may not be needed, but instead, a few points in depths may be sufficient, such as for sensing or in cases where a few *en-face* OCT images only would be needed.

3) *Increasing the number of depths addressed:* If OO DLF is too bulky to extend the number of LIs to large numbers, such as over 100, then only integrated optics may do it. However, at the current level of technology, EO DLF has more chances in this respect, where integrated electronics may be more feasible than integrated optics. Having 100 processors for 100 depths, then even an A-scan with 100 points can be produced in a time interval commensurate with sweeping time. If this would be feasible, then, such a method can be used to deliver not only *en-face* images,

but A-scans in the time interval of a sweep, whatever short. Photodetectors and *I&Q* mixers exist for tens of GHz operation.

4) *Bidirectional sweeping:* There is an active line of research on SSOCT. A recent direction to mention is that of bidirectional sweeping [15], where the OO regime of DLF was proven useful in producing interlaced *en-face* OCT images using both sweeps with a much simplified signal processing than performing FFT based OCT processing on each sweep direction. The OO DLF method reported [15] can equally be replicated by the EO DLF, where each mask stored is made of two masks, for forward sweeping continuing in time with the modulation during the back sweeping interval.

VI. Discussions and Conclusion

According to our results, a comparison of conventional FFT based OCT with different LF OCT modalities is presented in Table I.

Advantages and disadvantages of electrical versus optical production of signals to perform Downconversion Leader-Follower process have been presented. The AWG had a restricted bandwidth and experiments could only be done up to the OPD values that produce frequencies within the bandwidth of the synthesizer AWG. However the axial range was large enough to perform comparative characterization between the OO and EO cases and draw important conclusions on the value of such an approach. The procedure described here can be assimilated to an individual calculation of each z component of a complex LF transformation in (2), where the periodic chirped factor for a given z is synthesized by an AWG.

Replacing the optical generation of masks with electrical generation presents the disadvantage of periodic calibration needed, if the tuning curve, *g(k)*, varies in time. Such effects have already been documented [5], [15]. This is a disadvantage as well as for conventional OCT method, employing resampling followed by FFT. This is also a disadvantage for the digital CLF OCT systems that calculate the masks, when operating without a clock signal. OO DLF using a LI is tolerant to such fluctuations in the tuning profile as the mask is generated in real time according to the same *g(k)* in both interferometers that are driven by the same swept source. The OO DLF using one or more LIs would secure tolerance to *g(k)* shape variation. This tolerance to *g(k)* variation is similar to that employed in the conventional SSOCT signal processing using the clock signal produced by a clock circuit in the swept source. On the other hand, a further advantage of the EO DLF is that the masks generated by the AWG are characterized by the same *h(k)* as that affecting the channeled spectrum in the FI. Hence the mask synthesized incorporates the same dispersion as in the FI, which supposedly is not subject to temporal fluctuations like *g(k)*. The OO case presents the disadvantage of differences in the dispersion of the two interferometers. While we are working on a solution to reduce the effects of *g(k)* profile variation, it may be possible in the near future to devise tuning lasers with tuning profile more stable over time, facilitating the EO DLF applications. Adoption of EO DLF will depend on lowering the cost of GHz AWGs. There are several companies selling input boards up to a few GS/s while offers of similar sampling rate output boards (to perform the function of the AWG) are only a few and for a much higher price. The AWG instrument identified as a possible candidate for EO downconversion presented here, a Moku:Pro device from Liquid Instruments, is only one of two options found on the market, the other one, from Active Technologies, being much more expensive. The high demand by the OCT community for input boards lead to reduction of input digitiser prices, while so far there was no need for an AWG in OCT. We believe that with this report, the demand for AWGs in OCT will increase.

As for the *I&Q* mixer employed here, this is an active field of research, with reports operating at over 100 GHz [23]. Therefore such devices are ideally suited to process the many tens of GHz photodetected signals as delivered by ultra fast SSOCT systems. For sure, OO DLF, i.e., configurations using optical generation of masks have a future, as DLF eliminates the need of high sampling rates digitizers. EO DLF however needs not only high speed *I&Q* mixers, but synthesizers. As already commented above, it may be possible, by compromising slightly the axial resolution, to produce an approximate mask using low cost oscillators, instead of employing multi GHz digital synthesizers. Such low cost solutions should be capable of generating a chirp sufficiently close to that needed. In any case, at the extreme, simple sinusoidal generators would not work. If the cost of such synthesizer can be reduced to that of a balanced detector ($\sim$ \$5k) for the multi tens of GHz, then EO DLF solution is of less cost than the OO DLF. As for the I&Q mixers, passive or active they are in the range of 100-300 \$, i.e., not expensive.

Acknowledgment

The authors would like to thank Mark Hathaway for the software displaying two interlaced *en-face* images.

The author Alejandro Martinez Jimenez has devised the AWG software controls. The author Ramona Cernat acquired the experimental data. The authors Alejandro Martinez Jimenez and Ramona Cernat worked jointly on the graphics of the presentation. Adrian Podoleanu devised the concept of the paper and the frame of presentation. All authors contributed to the collation and organization of presentation of the study.

Disclosures: Adrian Podoleanu is inventor and coinventor of patents in the name of the University of Kent. No other conflict of interest.

Data Availability: Data underlying this study are available from the authors upon reasonable request.

References

[1] W. Drexler and J. G. Fujimoto, Eds., *Optical Coherence Tomography: Technology and Applications*. Berlin, Germany: Springer-Verlag, 2008.

[2] S. R. Chinn, E. A. Swanson, and J. G. Fujimoto, "Optical coherence tomography using a frequency-tunable optical source," *Opt. Lett.*, vol. 22, no. 5, pp. 340–342, Mar. 1997, doi: 10.1364/OL.22.000340.

[3] A. G. Podoleanu and A. Bradu, "Master–slave interferometry for parallel spectral domain interferometry sensing and versatile 3D optical coherence tomography," *Opt. Exp.*, vol. 21, no. 16, pp. 19324–19338, 2013, doi: 10.1364/oe.21.019324.

[4] S. Rivet, M. Maria, A. Bradu, T. Feuchter, L. Leick, and A. Podoleanu, "Complex master slave interferometry," *Opt. Exp.*, vol. 24, no. 3, pp. 2885–2904, 2016, doi: 10.1364/oe.24.002885.

[5] A. Podoleanu, R. Cernat, and A. Bradu, "Down-conversion en-face optical coherence tomography," *Biomed. Opt. Exp.*, vol. 10, no. 2, pp. 772–788, 2019, doi: 10.1364/boe.10.000772.

[6] R. Cernat, A. M. Jimenez, and A. Podoleanu, "Downconversion master slave optical coherence tomography for simultaneous en-face imaging at two depths," *Opt. Exp.*, vol. 32, no. 17, pp. 30756–30774, Aug. 2024, doi: 10.1364/OE.530325.

[7] S. Makita, T. Fabritius, and Y. Yasuno, "Full-range, high-speed, high-resolution 1-μm spectral-domain optical coherence tomography using BM-scan for volumetric imaging of the human posterior eye," *Opt. Exp.*, vol. 16, no. 12, pp. 8406–8420, Jun. 2008, doi: 10.1364/OE.16.008406.

[8] D. M. Pozar, *Microwave Engineering*, 4th ed. Hoboken, NJ, USA: Wiley, 2012.

[9] G. Yu, D. ChangHao, L. GuoDong, L. BingGuo, C. FengDong, and L. BingHui, "Continuous dynamic measurement of frequency scanning interferometry based on motion phase synchronization compensation and calibration," *Opt. Exp.*, vol. 31, no. 19, pp. 30974–30992, Sep. 2023, doi: 10.1364/OE.497770.

[10] A. Bradu et al., "Recovering distance information in spectral domain interferometry," *Sci. Rep.*, vol. 8, no. 1, 2018, Art. no. 15445, doi: 10.1038/s41598-018-33821-0.

[11] N. Lippok, S. Coen, P. Nielsen, and F. Vanholsbeeck, "Dispersion compensation in Fourier domain optical coherence tomography using the fractional Fourier transform," *Opt. Exp.*, vol. 20, no. 21, pp. 23398–23413, Oct. 2012, doi: 10.1364/OE.20.023398.

[12] X. Zhang et al., "Optical computing for optical coherence tomography," *Sci. Rep.*, vol. 6, no. 1, Nov. 2016, Art. no. 37286, doi: 10.1038/srep37286.

[13] R. Cernat et al., "Gabor fusion master slave optical coherence tomography," *Biomed. Opt. Exp.*, vol. 8, no. 2, pp. 813–827, 2017, doi: 10.1364/boe.8.000813.

[14] J. P. Fingler, "Motion contrast using optical coherence tomography," Ph.D. dissertation, California Inst. Technol., Pasadena, CA, USA, 2007.

[15] A. M. Jimenez et al., "Downconversion master slave OCT with a bidirectional sweeping laser," *J. Biophotonics*, vol. 18, no. 12, 2025, Art. no. e202400201, doi: 10.1002/jbio.202400201.

[16] M. R. Di Nicola, M. Colombo, G. E. N. Kass, G. Paolino, P. N. Strong, and J. L. C. M. Dorne, "Scorpions: Taxonomy, anatomy, medical relevance, venom composition, pharmacology, toxicology and clinical management," in *Encyclopedia of Toxicology*. Amsterdam, The Netherlands: Elsevier, 2024, pp. 445–456, doi: 10.1016/B978-0-12-824315-2.00209-8.

[17] R. Mullen and W. D. Sissom, "Chapter 23 - scorpions," in *Medical and Veterinary Entomology*, 3rd ed. London, U.K.: Academic Press, 2019, pp. 489–504.

[18] R. Stockmann, "Introduction to scorpion biology and ecology," in *Scorpion Venoms*. Berlin, Germany: Springer-Verlag, 2015, pp. 25–59, doi: 10.1007/978-94-007-6404-0_14.

[19] A. M. Jimenez, S. Grelet, V. Tsatourian, P. B. Montague, A. Bradu, and A. Podoleanu, "400 Hz volume rate swept-source optical coherence tomography at 1060 nm using a KTN deflector," *IEEE Photon. Technol. Lett.*, vol. 34, no. 23, pp. 1277–1280, Dec. 2022, doi: 10.1109/LPT.2022.3212015.

[20] I. Akkaya and S. Tozburun, "A 1060 nm stretched-pulse mode-locked wavelength-swept laser source providing an A-scan rate of 20 MHz," *Optik*, vol. 266, Sep. 2022, Art. no. 169648, doi: 10.1016/j.ijleo.2022.169648.

[21] Z. Wang et al., "Cubic meter volume optical coherence tomography," *Optica*, vol. 3, no. 12, pp. 1496–1503, Dec. 2016, doi: 10.1364/OPTICA.3.001496.

[22] M. Marques, R. Cernat, J. Ensher, A. Bradu, and A. Podoleanu, "Akinetic swept-source master–slave-enhanced optical coherence tomography," *Photonics*, vol. 8, no. 5, Apr. 2021, Art. no. 141, doi: 10.3390/photonics8050141.

[23] L. Mullen, A. Laux, B. Cochenour, E. P. Zege, I. L. Katsev, and A. S. Prikhach, "Demodulation techniques for the amplitude modulated laser imager," *Appl. Opt.*, vol. 46, no. 30, pp. 7374–7383, Oct. 2007, doi: 10.1364/AO.46.007374.